Dissociative ionization of OCS induced by highly charged ion impact

Bo Wang,[1] Jie Han,[1] Xiaolong Zhu,[2,*] Long Wei,[1] Baihui Ren,[1] Yu Zhang,[3] Wandong Yu,[1] Shuncheng Yan,[2] Xinwen Ma,[2] Yaming Zou,[1] Li Chen,[1] and Baoren Wei[1,†]

[1]*Institute of Modern Physics, Key Laboratory of Nuclear Physics and Ion-Beam Application (MOE), Fudan University, Shanghai 200433, China*

[2]*Institute of Modern Physics, Chinese Academy of Sciences, Lanzhou 730000, China*

[3]*School of Mathematics, Physics and Information Engineering, Jiaxing University, Jiaxing 314001, China*

(Received 18 November 2020; accepted 25 March 2021; published 7 April 2021)

Dissociation of OCS^{q+} ($q = 3$–7) produced by 18-keV/u Ne^{8+} ion impact has been investigated using recoil ion momentum spectroscopy. Ten complete three-body Coulomb fragmentation channels were analyzed. Scattered projectile charge state (Ne^{7+} or Ne^{6+}) differentiated branching ratios and the kinetic-energy release (KER) distributions were analyzed for different fragmentation channels. Through Dalitz plots, Newton diagrams, and native frames, we have studied the concerted and sequential fragmentation mechanisms for channels leading to $O^+ + C^+ + S^+$, $O^+ + C^+ + S^{2+}$, $O^{2+} + C^+ + S^+$, and $O^+ + C^+ + S^{3+}$. For concerted dissociation mechanisms, the molecular bending fragmentation dominates in these channels. For sequential dissociation mechanisms, the KER distribution for the dissociation of intermediate ions CO^{2+}/CS^{2+} were determined and the rotation of the intermediate molecular ion CO^{2+} before the second step dissociation was discussed. Thereby the relative branching ratios of events coming from sequential versus concerted mechanism were also estimated.

DOI: 10.1103/PhysRevA.103.042810

I. INTRODUCTION

The dissociation of multiply ionized molecules has been a very active area of research for its fundamental and application importance, such as plasma physics [1] and planetary atmospheric chemistry [2,3]. The ionization of triatomic molecules results, in most cases, in transitions to excited states of the molecular ions and eventually leads to dissociation via two-body or three-body fragmentation pathways, showing interesting dynamics [4–7]. For example, the three-body fragmentation (three ionic fragments) of polyatomic molecular ions can proceed via one-step (concerted) or two-step (sequential) processes, depending on the time delay between two bond cleavages. Meanwhile, in the process of fragmentation, some of the excessive energy of excited molecule states is released as the kinetic energy of the fragments. Thus, the determination of the kinetic-energy release (KER) contains rich dissociation dynamics information. With the cold target recoil ion momentum spectroscopy (COLTRIMS) [8], the fragmentation mechanism can be identified more clearly and convincingly by analyzing the momentum correlation and angular information of all resultant fragments. Recently, there are many works to study the fragmentation mechanism of a molecule with the Dalitz plots, Newton diagrams, and native frames [9–13].

OCS is important in the global cycling of sulfur and has been discovered in the atmosphere, volcanic gases, ice cores in Antarctica, and the interstellar medium [14]. A lot of effort has been directed to studying the ionization and fragmentation of OCS induced by intense lasers [12,15–19]. Sanderson *et al.* [15] studied the Coulomb explosion of OCS in laser pulses and proposed a classical enhanced ionization model to explain their observation. The kinetic-energy release during two- and three-body Coulomb explosions of OCS induced by 790-nm 50-fs laser pulses [16] has been measured using three-dimensional (3D) covariance mapping, and it was observed that OCS^{3+} dissociated into two distinct energy channels giving $C^+ + O^+ + S^+$ iontriplets. Brites *et al.* [17] made multireference configuration interaction calculations of a number of electronic states of the OCS^{2+} to examine kinetic-energy releases. Wales *et al.* [18] reported the concerted and sequential dissociation mechanisms of OCS^{3+} and OCS^{4+}. They found that for increasing pulse length (from 7 to 200 fs), the concerted three-body dissociation exhibited increasing bending and the amount of sequential dissociation events decreased, however, for 200 fs, the count of the stepwise process increased again. By using the energy selected Auger electron-photoion-photoion coincidence, Saha *et al.* [19] investigated the state-selected fragmentation mechanism of OCS^{2+}. Recently, Rajput *et al.* [12] have employed the native frame to separate sequential from concerted breakup for OCS^{3+}, even when their signals overlapped. This native frame applicable for any projectile (electrons, ions, or photons) provides detailed information on each step of the sequential breakup. In the aspect of electron collision [20,21], Wang and Vidal [20] reported the dissociation of multiply ionized carbonyl sulfide using two- and three-dimensional covariance mapping techniques. The fragmentation dynamics of OCS after double, triple, and quadruple ionizations by electron collision at 500 eV was investigated by Shen *et al.* [21]. Compared

*zhuxiaolong@impcas.ac.cn
†brwei@fudan.edu.cn

to photoionization, the work on highly charged ion (HCI) impact [13,22–24] ionization of OCS is rather limited. Recently, the fragmentation dynamics of OCS induced by HCI collision has been studied by Jana and co-workers using fast ions (150-keV Ar^+ and 5-MeV/u Si^{12+}) [22,23]. From the coincidence map of the fragments, Jana and co-workers have separated complete two- and three-body (two ionic and one neutral fragment) dissociation channels of OCS^{q+} ($q = 2$–4). A native frame based on the angular correlation of fragments has been used by Kumar *et al.* [13] to check for an active sequential mechanism in the three-body breakup of OCS^{3+} using 1.8-MeV Xe^{9+}. Wales *et al.* [24] used Ar^{4+} and Ar^{8+} projectile impact at 15 keV/q, which applied the ion impact and coincidence momentum imaging technique. The breakup of OCS from 2+ up to 6+ and compared the experimental KER with theoretical values simulated from the Coulomb explosion. Furthermore, they are focused on the fragmentation mechanism of OCS^{3+} ions and found the generation of a CO^{2+} over a CS^{2+} metastable by a ratio 5/2.

In the present paper, we report on systematic investigations of three-body dissociation of multiply charged OCS^{q+} ($q = 3$–7) induced by 18-keV/u Ne^{8+} impact. The scattered projectile charge state differentiated branching ratios will be presented for ten three-body dissociation channels identified in our experiment. Using the COLTRIMS, the KER distribution for each channel was determined. Dissociation mechanisms of the main channels leading to $O^+ + C^+ + S^+$, $O^+ + C^+ + S^{2+}$, $O^{2+} + C^+ + S^+$, and $O^+ + C^+ + S^{3+}$ will be further analyzed using the Dalitz plots, Newton diagrams, and native frames. Both concerted and sequential dissociation processes are observed for each of the above channels. The molecular bending of OCS^{3+} and OCS^{4+} at the moment of concerted dissociation and the rotation of the CO^{2+} intermediate ion before the second step dissociation will be discussed.

II. EXPERIMENTAL SETUP

The experiment was conducted on the highly charged ion collision platform at Fudan University in Shanghai. It mainly consists of a permanent-magnet 14.5-GHz electron cyclotron resonance ion source and a COLTRIMS setup. The details of the experimental setup have been described in previous publications [25]. In brief, an 18-keV/u Ne^{8+} beam crossed a cold target jet produced by a OCS gas at 1 bar escaping through a 20-μm nozzle into the vacuum chamber. After an interaction, the target molecule could undergo dissociative ionization and give rise to various fragmentation processes involving C-O and/or C-S bond cleavages leading to two or three fragments. Fragment ions in the interaction zone were extracted by a static electric field of 220 V/cm, which ensured that ions with kinetic energy of less than 20 eV were collected in a 4π solid angle. The recoil ions flying through the acceleration section of 10 cm in length and a field-free section of 20 cm were detected by a position sensitive detector equipped with two multichannel plates of 75 mm in diameter. Meanwhile, the scattered projectiles passing through a parallel plate-electrostatic analyzer were recorded by another position-sensitive detector. They were differentiated in the charge state according to their position on the detector. In the present experiment, scattered projectile ions Ne^{7+} and Ne^{6+} were dominant, whereas a small amount of Ne^{5+} and Ne^{4+} ions were also observed. For each event, the scattered ion signal served as the time reference for the time of flight (TOF) measurements of the associated ionic fragments. Finally, based on the TOF and the corresponding position data recorded by the position-sensitive detector, the 3D momentum vectors for each recoil ion were constructed.

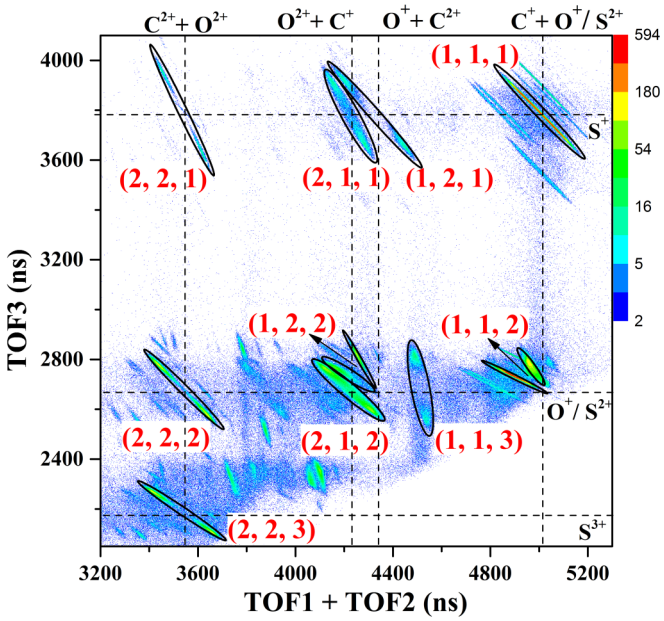

FIG. 1. Triple ion coincidence TOF map resulting from the OCS^{q+} ($q = 3$–7) dissociation caused by 18-keV/u Ne^{8+} impact. The charge of the scattered projectile ions is not differentiated for Ne^{r+} ($r = 4$–7).

III. RESULT AND DISCUSSION

A. Relative branching ratios of three-body dissociation channels of OCS^{q+} ($q = 3$–7)

Three-body Coulomb explosion channels resulting from the dissociation of OCS^{q+} ($q = 3$–7) induced by 18-keV/u Ne^{8+} impact are observed. In the following, a dissociation channel is labeled (a, b, and c) according to the convention $OCS^{(a+b+c)+} \rightarrow O^{a+} + C^{b+} + S^{c+}$. There are ten dissociation channels identified in the triple ion coincidence TOF map shown in Fig. 1: (1, 1, 1), (1, 1, 2), (2, 1, 1), (1, 2, 1), (1, 1, 3), (2, 1, 2), (1, 2, 2), (2, 2, 1), (2, 2, 2), and (2, 2, 3). In order to illustrate the coincident measurement of three charged fragments, the sum of the TOFs of the first and second detected ions TOF1 + TOF2 is plotted along the horizontal axis, whereas that of the third detected ion TOF3 is plotted along the vertical axis. Each ellipse surrounded by a black elliptic line on the coincidence map is related to a simultaneous detection of three ions. The ellipses at the top of the map for TOF3 around 3800 ns correspond to channels with the detection of a S^+ fragment. The two parts of an ellipse above or below the line defined by the nominal TOF of S^+ are related to dissociation events when S^+ is emitted backward or toward, respectively, the TOF tube. Near channel (1, 1, 1), there are some other ellipses with much

TABLE I. Branching ratios of three-body dissociation channels of OCS^{q+} ($q = 3$–7) by Ne^{8+} impact taken without differentiation of the scattered projectile charge state Ne^{r+} ($r = 4$–7) and in coincidence with Ne^{6+} and Ne^{7+}. Measured kinetic-energy release for three-body dissociation channels of OCS^{q+} ($q = 3$–7) together with the predictions by the CEM.

	Branching ratio (%)		KER (eV)		
Channels	Ne^{r+} ($r = 47$)	Ne^{7+}	Ne^{6+}	Experimental	CEM
(1, 1, 1)	15.1	11.6	3.4	18.0/24.0	27.0
(1, 1, 2)	39.7	16.0	20.2	38.3	41.5
(2, 1, 1)	2.0	0.5	1.3	42.0	44.7
(1, 2, 1)	2.3	0.7	1.4	43.5	48.6
(1, 1, 3)	0.9	0.1	0.7	58.5	56.0
(2, 1, 2)	8.3	0.8	6.6	65.5	64.5
(1, 2, 2)	14.7	1.5	12.0	66.4	72.4
(2, 2, 1)	1.4	0.1	1.1	71.4	78.8
(2, 2, 2)	8.1	0.2	5.9	98.6	107.9
(2, 2, 3)	7.6	0.1	4.0	126.6	136.9

lower statistics due to the isotopes of ^{13}C, ^{33}S, and ^{34}S. The ellipses for TOF3 around 2680 ns correspond to channels with the detection of a S^{2+} or (and) an O^+. The TOFs of O^+ and S^{2+} are degenerated. When both ions are involved in a dissociation event as in the case of channels (1, 1, 2) and (1, 2, 2), two coincidence ellipses above the nominal TOF of O^+/S^{2+} with different slopes are observed for each channel. This is due to the fact that for these two channels, the last ion arriving at the detector associated with TOF3 corresponds surely to one of the ions O^+ or S^{2+} emitted backward the TOF tube. The momentum vector P of each ion is deduced from the observed TOF T : $P_{\mathrm{TOF}} = qE(T_0 - T)$ [21], where q is the ion charge and E is the extraction field. T_0 is the central value of TOF corresponding to the ions with zero momentum along the extraction axis. In the experiment, O^+ and S^{2+} have an initial momentum. The slope of an ellipse is only sensitive to the charge of the last detected ion. These results in the special tweezers structure of the corresponding ellipses in the TOF map.

In Fig. 1, one can note ten three-body fragmentation channels for OCS^{q+} ($q = 3$–7). In principle, the relative branching ratio of each channel could be obtained by the count of the corresponding ellipse divided by the total count of the ten channels. However, due to the incomplete collection or finite angular acceptance for ions with kinetic energy larger than 20 eV under the present experimental condition, some energetic ionic fragments with a large translational velocity component with respect to the TOF axis are not collected. This leads to the characteristic structure of most of the ellipses in Fig. 1. As an example, for channel (1, 2, 1), the count is larger in the vicinity of both ends of the ellipse, corresponding to events when fragment ions are ejected along the TOF axis or in a small angle to the TOF axis. Whereas, the count is negligible in the middle part of the ellipse, corresponding to events when the ions are ejected with a larger angle to the TOF axis. Using the standard COLTRIMS methodology, we have determined the three-dimensional momenta of all ionic fragments for each dissociation event. Based on the assumption that the emission angles of the ions are isotropic. To extract the branching ratios, an angle restriction for the momenta of ions is applied during the data processing. For example, an angle of less than 20 ° toward or backward from the TOF axis can avoid the energetic ion losses, thus, ensuring the reasonableness of the assumptions. With this restriction, all recoil ions could be collected in 100%, and the ion pair loss due to the dead time of the detector could be also avoided, for example, in dissociation channels involving O^+ and S^{2+}. The branching ratios of three-body dissociation without differentiation of the scattered projectile charge for Ne^{r+} ($r = 3$–7) are then obtained and listed in Table I. In this paper, the relative uncertainty, about 20% for each value, is mainly contributed by the data statistics and the detection efficiency.

The total three-body dissociation branching ratios for OCS^{q+} with q varying from 3 to 7 are found to be about 15.0%, 44.0%, 25.3%, 8.1%, and 7.6%, respectively. The maximum contribution comes from OCS^{4+}. It is well known that in ion-molecular target collisions at intermediate velocity (v on the order of 1 a.u.), both electron capture and direct ionization take place and the cross section decreases with increasing number of electrons removed from the target [26]. Therefore, one should expect that the population of OCS^{q+} produced due to Ne^{8+} impact decreases with increasing charge q. The contribution of OCS^{3+} to the three-body dissociation is relatively low. The reason is that the dominant dissociation process of OCS^{3+} is the two-body fragmentation (such as $CO^{2+} + S^+$, $CS^{2+} + O^+$, etc.).

Triple ion coincidence TOF maps are also built in coincidence with the selective scattered projectile charge state Ne^{7+} or Ne^{6+}. Using the same data analysis procedure as described above, the count corresponding to each channel is obtained. The related branching ratio, defined as the count of a projectile charge selected channel divided by the total count of all three-body fragmentation channels without differentiation of the scattered projectile charge are obtained for Ne^{7+} and Ne^{6+} and listed in Table I. One can note that the three-body fragmentation channel (1, 1, 1) was contributed in the major part by one-electron-capture collisions (Ne^{7+} for 11.6%) and in the smaller part by two-electron-capture collisions (Ne^{6+} for 3.4%). For quadruply charged molecules OCS^{4+}, the three-body dissociation channels (1, 1, 2), (2, 1, 1), and (1, 2, 1) are contributed by one- or two-electron-capture collisions with comparable branching ratios, about 17% for Ne^{7+} and 23%

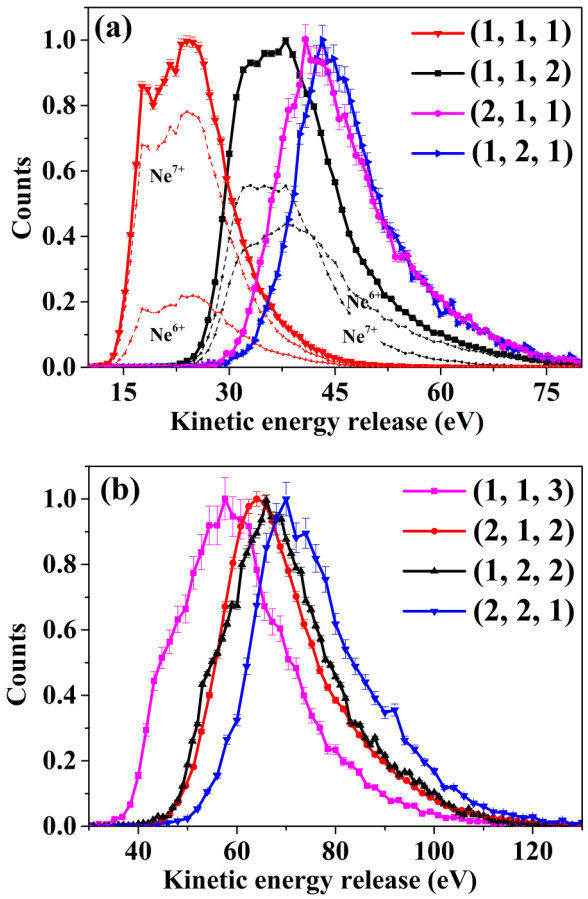

FIG. 2. (a) and (b) KER distribution for three-body dissociative channels of OCS^{q+} ($q = 3$–5) without differentiation of the scattered projectile charge state Ne^{r+} ($r = 4$–7) (solid line). (a) Dotted lines: KER distributions for channels (1, 1, 1) and (1, 1, 2) in coincidence with Ne^{6+} or Ne^{7+}.

for Ne^{6+}. For OCS^{5+}, the three-body dissociation channels (1, 1, 3), (2, 1, 2), (1, 2, 2), and (2, 2, 1) are contributed mainly by two electron capture collisions, 20.4% for Ne^{6+}, whereas only 2.5% for Ne^{7+}. For highly charged molecules OCS^{q+} ($q = 6, 7$), the three-body dissociation channels (2, 2, 2) and (2, 2, 3) are related mostly to Ne^{6+} or other lower charge states Ne^{r+} ($r < 6$).

B. KER spectra for three-body fragmentation of OCS^{q+} ($q = 3$–7)

For each three-body dissociation event, the KER of the corresponding dissociation process is determined from the momenta of all involved charged fragments obtained with the COLTRIMS. The center-of-mass (c.m.) is used in reconstructing the fragment momentum. The KER distributions for ten three-body fragmentation channels are drawn, and the peak values are listed in Table I. The uncertainty of the KER value in the present paper mainly comes from the resolution of the momentum spectrometer and uncertainty of the data statistics, which are about 0.5 eV. The KER distributions are presented in Fig. 2(a) for parent molecular ions OCS^{q+} ($q = 3, 4$) and in Fig. 2(b) for OCS^{5+}. For channel (1, 1, 1), one can note a maximum of the KER distribution at about 24 eV and a narrow peak at lower energy around 18 eV. The main peak is in agreement with ~24 eV of Jana *et al.* [23] using Si^{12+} ions, whereas the low-energy peak is similar to that of Wales *et al.* [18] by the strong-field laser. The structure with double components observed in our experiment indicates that both high- and low-excitation energy states are populated for OCS^{3+} parent ions in collisions with Ne^{8+} at 18 keV/u. The KER distributions measured in coincidence with Ne^{7+} and Ne^{6+} are presented in the Fig. 2(a) and show similar structures. This suggests that the excitation energy distribution of OCS^{3+} prepared in one- or two-electron-capture collisions is quite comparable.

For the three-body fragmentation channels of OCS^{4+}, three KER distributions are presented in Fig. 2(a). The distribution for channel (1, 1, 2) appears wider than the other two channels (2, 1, 1) and (1, 2, 1). The KER distributions of the (1, 1, 2) channel differentiated by the final charge of projectiles Ne^{7+} and Ne^{6+} show two distinct curves with comparable counts centered around 35 and 39 eV, respectively, in Fig. 2(a). The cross section of one-electron capture is much larger than that of two-electron capture, indicating that the collision parameter of the two-electron-capture process is smaller and the collision is more intense. This makes the OCS^{4+} corresponding to Ne^{6+} on higher excited states, resulting in a larger KER peak value. A tail extended to the higher-energy range can be also noted for the distribution related to Ne^{6+}. Therefore, we can see that OCS^{4+} parent ions undergoing three-body dissociation (1, 1, 2) are prepared with a broader excitation energy distribution contributed at lower energy by one-electron-capture collisions and at slightly higher energy by two-electron-capture collisions. Meanwhile, for channels (2, 1, 1) and (1, 2, 1), the contribution from collisions related to Ne^{7+} is found much lower than that related to Ne^{6+} (see Table I) and the KER distributions are accordingly narrower than for channel (1, 1, 2). Comparing with previous experiments using laser ionization, the KER distribution range in the current experiments is found significantly wider, and the KER peak is larger. The peak values of KER for channel (1, 1, 2) measured in the present paper are much larger than the values obtained by Bryan *et al.* [16] (18 eV) and Ma *et al.* [27] (20 eV). We hypothesize that these low-energy values could be attributed to the molecular structure deformation in the intense laser field before the Coulomb explosion. For the dissociation of OCS^{5+}, significant differences can also be noted for the same reason. A small KER peak value of 34 eV is measured by the above two groups for channel (1, 2, 2), whereas, in the present paper, we found a larger value of 66 eV. Despite the very different excited-state population of OCS^{q+} ($q = 4, 5$) compared with laser excitation experiments, the KER peak values of most of channels (1, 1, 2), (2, 1, 1), (1, 2, 1), and (2, 1, 1) measured in this paper are in good agreement with the results obtained by Wales *et al.* [24] in the HCl collision and Shen *et al.* [21] in electron impact. So, the ionization and excitation mechanism plays an important role in the energy distribution of OCS^{q+} and, consequently, in the dissociation of the molecular ions. Comparable energy ranges are found for dissociation channels in experiments using HCI and electron impact. For highly charged ions OCS^{6+} and OCS^{7+}, the dominant three-body fragmentation channels (2, 2, 2) and (2, 2, 3), respectively, are analyzed. The KER distributions are not presented here, but the peak values are listed in Table I.

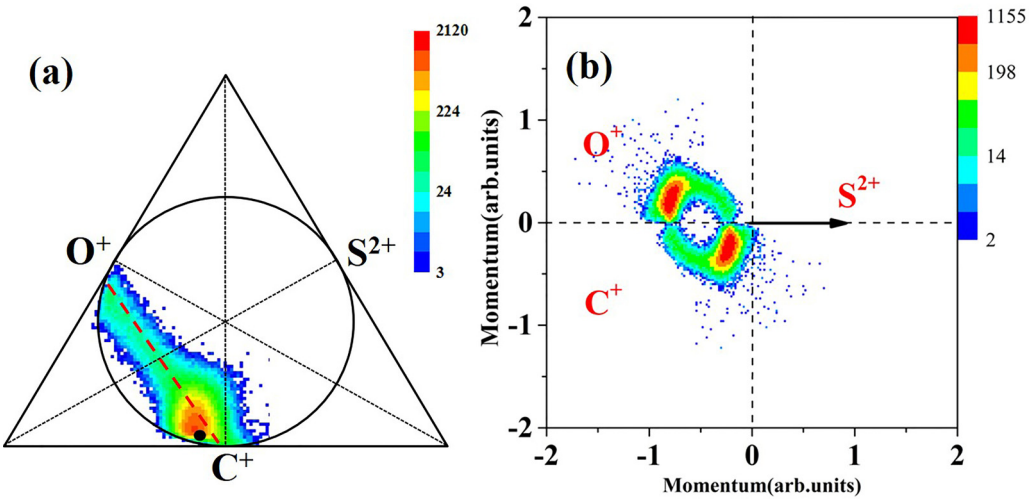

FIG. 3. (a) Dalitz plot and (b) Newton diagram for channel (1, 1, 2). The momentum of O^+, C^+, and S^{2+} in the concerted dissociation process of a linear OCS^{4+} is simulated by CEM, and the corresponding point is drawn in the Dalitz plot (the black dot). The slope of the winglike structure also was simulated by CEM (red dashed line).

To compare with the measured KER peak values, we have estimated the kinetic-energy release for each dissociation channel using a simple CEM [28]. In this model, a molecular ion of linear structure is supposed to be composed of three ions O^{a+}, C^{b+}, and S^{c+} at their initial positions separated by the average lengths R of the bonds of a neutral OCS ($R_{C-O} \sim 1.16$ Å and $R_{C-S} \sim 1.56$ Å). To simulate the dissociation, all molecular bonds are considered to break simultaneously, and the fragment ions are driven apart purely by their Coulomb repulsive force. The obtained values are listed in Table I. Despite the roughness of the model, the CEM values follow quite well the evolution of the KER values, the KER peak value increases with the increasing charge of OCS^{q+}, and for a given charge state, the variation of the KER according to the distribution of the charge on the molecule.

C. The dissociation mechanisms of three-body channels for OCS^{q+} (q = 3–7)

Three-body fragmentations of OCS^{q+} involve the break of two bonds, the O-C and C-S bonds. In the following, we are interested in the dissociation mechanism of OCS^{q+}, the concerted dissociation, i.e., the simultaneous break of the two bonds and the sequential dissociation, i.e., the break of the two bonds in two steps. For each channel, the momentum correlation and angular information of fragment ions will be analyzed in detail in order to extract the information concerning the dissociation mechanisms.

1. *Concerted dissociation and sequential breakup of* OCS^{3+} *and* OCS^{4+} *via* $CO^{2+} + S^+$ *and* $CO^{2+} + S^{2+}$

The Dalitz plot provides a powerful tool to visualize the momentum correlation of resultants and, thus, to identify the dissociation mechanisms [9–11]. Briefly, considering a dissociation channel (a, b, or c), for each dissociation event, using the momenta p_i, i = 1–3 obtained with COLTRIMS for the corresponding fragment ions O^{a+}, C^{b+}, and S^{c+}, we have calculated the normalized momentum square values defined as $\varepsilon_i = p_i^2/\Sigma p_i^2$. According to the conservation of momentum, in a Dalitz plot, the data are plotted within a circle inscribed in an equilateral triangle. Put the center of the circle at the origin of the Cartesian coordinates, then the x and y axes in the Dalitz plot are defined as $x = (\varepsilon_1 - \varepsilon_3)/\sqrt{3}$ and $y = \varepsilon_2 - 1/3$. Here, each event is represented by a point (ε_1, ε_2, and ε_3) plotted within a circle of radius 1/3 inscribed in an equilateral triangle. Each side of the triangle with the fragment in the process is an axis label i.e., O^{a+}, C^{b+}, and S^{c+}. The vertical distance of an event point from each edge equals the value of ε_i calculated for the corresponding fragment.

For dissociation channel (1, 1, 2), the Dalitz plot is built and shown in Fig. 3(a). In this figure, one can note first an intense spot near the bottom edge (C^+) of the triangle. For events in this area, the momentum of C^+ is much smaller than those of the other two fragments showing a typical feature of concerted dissociation of OCS^{4+}. For a linear structure, C^+ in the middle of the molecule, pushed by O^+ and S^{2+} from both sides, should receive little momentum during the dissociation. Using the CEM, we have calculated the momenta of O^+, C^+, and S^{2+} obtained in a concerted dissociation process of a linear OCS^{4+}. The corresponding point is drawn in the Dalitz plot (the black dot). For OCS^{4+} with a bending structure, C^+ should gain slightly larger momentum during the dissociation leading to a shift of the event points above the black dot in the region of the intense spot. Therefore, this intense spot is attributed to the concerted dissociation process where all bonds break simultaneously. In Fig. 3(a), one can note another area, the left-winglike structure extending from the edge (C^+) to the edge (O^+). For events in this area, the momentum of S^{2+} varies slowly, whereas the momenta of C^+ and O^+ show a strong correlation. This feature is in agreement with the sequential dissociation process $OCS^{4+} \rightarrow S^{2+} + CO^{2+} \rightarrow O^+ + C^+ + S^{2+}$. In this process, the S^{2+} ion is lost by the molecule in a first step, and when the repulsion force between the escaping S^{2+} and CO^{2+} becomes negligible, the second bond breaks: $CO^{2+} \rightarrow C^+ + O^+$. The slope of the wing is simulated quite well with a sequential dissociation Coulomb model considering the rotation of the intermediate molecule CO^{2+} (the red dashed line in the Dalitz plot). Event

points near the edge (C^+) correspond to the cases when O^+ flies in the same direction as the intermediate parent CO^{2+} and C^+ in the opposite direction, those near the edge (O^+) correspond to the cases when C^+ flies in the direction of CO^{2+} and O^+ in the opposite direction, whereas event points at the middle of the wing correspond to the cases when the bond of CO^{2+} is perpendicular to the velocity of CO^{2+}. Therefore, this winglike structure is attributed without ambiguity to the sequential dissociation process, the break of the C-S bond at the first step followed by the break of the O-C bond via the intermediate fragment CO^{2+}. The metastable states of CO^{2+} have been widely investigated [29,30]. Its lifetime spans from submicroseconds to a few seconds, and those could be populated in the present experiment as two-body channels. For channel (1, 1, 2), another sequential dissociation process can be considered, i.e., the break of the O-C bond at the first step followed by the break of the C-S bond via the intermediate fragment CS^{3+}, $OCS^{4+} \rightarrow CS^{3+} + O^+ \rightarrow O^+ + C^+ + S^{2+}$. This process should lead to a right-winglike structure in the Dalitz plot, which is obviously absent in the Dalitz plot of Fig. 3(a). It indicates that the above sequential dissociation process is not observable in the present paper. The reason could be that there are usually no metastable states for triply charged diatomic ion CS^{3+}.

To see this more directly, the same data are displayed in a Newton diagram [9–11] in Fig. 3(b), wherein the momentum vector of S^{2+} is set as the unit vector along the x axis. The end points of the relative normalized momentum vectors of O^+ and C^+, respectively, are plotted above and below the x axis. The two intense spots along with two semicircular distributions correspond to the concerted and the sequential fragmentation mechanisms, respectively. The semicircular structures arise due to the rotation of the intermediate CO^{2+} molecular ion which acquires some angular momentum in the first breakup and rotates as it dissociates. The Newton diagram structure of other dissociation channels with the sequential dissociation process is similar to Fig. 3(b), so it will not be shown in the following.

To get more information on the fragmentation dynamics, a native frame based on a one-dimensional angular distribution proposed recently is used [12,13]. All events of channel (1, 1, 2) without differentiation of the concerted and sequential dissociation processes are analyzed in the same way. From the measured momentum vector of S^{2+}, $\vec{p}_{S^{2+}}$, we obtained the velocity vector of the c.m. for the ensemble of C^+ and O^+, equaling $\vec{v}_{\mathrm{c.m.}} = -\vec{p}_{S^{2+}}/(M_C + M_O)$. Using the measured momentum vectors, $\vec{p}_{O^+}$ and $\vec{p}_{C^+}$, the momentum vectors $\vec{p}'_{O^+}$ and $\vec{p}'_{O^+}$ in the c.m. frame reference are obtained. The corresponding velocities are presented in Fig. 4. Angle θ among $\vec{p}'_{O^+}$, $\vec{p}_{S^{2+}}$, and the kinetic energy of O^+ and C^+ in the frame reference c.m. called $E'(C^+, O^+)$ are then obtained. Each event is plotted in a two-dimensional spectrum according to $E'(C^+, O^+)$ and θ as shown in Fig. 5(a). The spot on the top of Fig. 5(a) is contributed by events corresponding to the intense spot in the Dalitz plot [Fig. 3(a)]. It is, therefore, attributed to the concerted dissociation. The vertical trail corresponding to events leading to the left-wing structure in Fig. 3(a) is attributed to two-step sequential dissociation via the CO^{2+} intermediate fragment. In addition, angular α distributions between momentum vectors of O^{a+} and S^{c+} ions for the concerted dissociation of channels (1, 1, 2), (2, 1, 1), (1, 2, 1), and (2, 1, 1) are shown in Fig. 6.

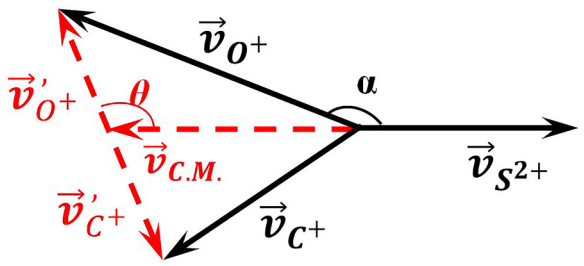

FIG. 4. Schematic of the kinematics of dissociation channel (1, 1, 2).

Figure 5(c) (the black line) is obtained by the projection of Fig. 5(a) on the θ axis. The main peak associated with the concerted dissociation is centered on ∼140°. The corresponding angle α between the momentum vectors of O^+ and S^{2+} ($\vec{p}_{O^+}$ and $\vec{p}_{S^{2+}}$) is found to be about 160° in Fig. 6. The value is smaller than the initial bending angle of the molecule at the moment of dissociation due to the Coulomb repulsion [6]. Although the geometry of the OCS molecule cannot be directly measured here, the momentum vectors give some indication of bending structure. It is obviously different from 180°, the angle expected for Coulomb explosion of a molecular ion with a linear geometry. It suggests that molecules OCS^{4+} prepared in collisions with 18-keV/u Ne^{8+} are brought most probably to excited states with a bending structure before the concerted dissociation. A similar process is observed in a previous work for CO_2^{3+} in collisions with 3.2-keV/u Ar^{8+} ions [9]. It is named asynchronous concerted dissociation to differentiate from the synchronous concerted dissociation where the molecules kept the linear structure as in the neutral ground state. However, in that previous work, the most likely configuration of the dissociating CO_2^{3+} is found to be linear, whereas in the present case, the contribution from COS^{4+} with linear structure is very small comparing to the bending structure.

Similarly, for channel (1, 1, 1), the Dalitz plot and the native frame are shown in Figs. 7(a) and 7(b), respectively. In Fig. 7(a), one can note the intense spot near the edge (C^+) corresponding to the concerted dissociation $OCS^{3+} \rightarrow O^+ + C^+ + S^+$, the left-winglike structure corresponding to the sequential two-step process $OCS^{3+} \rightarrow CO^{2+} + S^+ \rightarrow O^+ + C^+ + S^+$ via the CO^{2+} intermediate fragment and the right-winglike structure corresponding to the sequential dissociation process $OCS^{3+} \rightarrow CS^{2+} + O^+ \rightarrow O^+ + C^+ + S^+$ via the CS^{2+} intermediate fragment. To compare with the case of OCS^{4+}, we are interested in the sequential dissociation of OCS^{3+} via the intermediate CO^{2+}. Therefore, to draw Fig. 7(b), for each event, we have determined the momenta $\vec{p}'_{O^+}$ and $\vec{p}'_{C^+}$ in the c.m. frame reference of the ensemble of C^+ and O^+ and angle θ between $\vec{p}'_{O^+}$ and $\vec{p}_{S^+}$. The projection of Fig. 7(b) on the θ axis is presented in Fig. 7(c) (the black line). The main peak associated with the concerted dissociation is centered on about 135°. The corresponding angle α between the momentum vectors of O^+ and S^+ ($\vec{p}'_{O^+}$ and $\vec{p}_{S^+}$) is found to be about 160° in Fig. 6. It suggests that molecules OCS^{3+} prepared in the present experiment are brought most probably

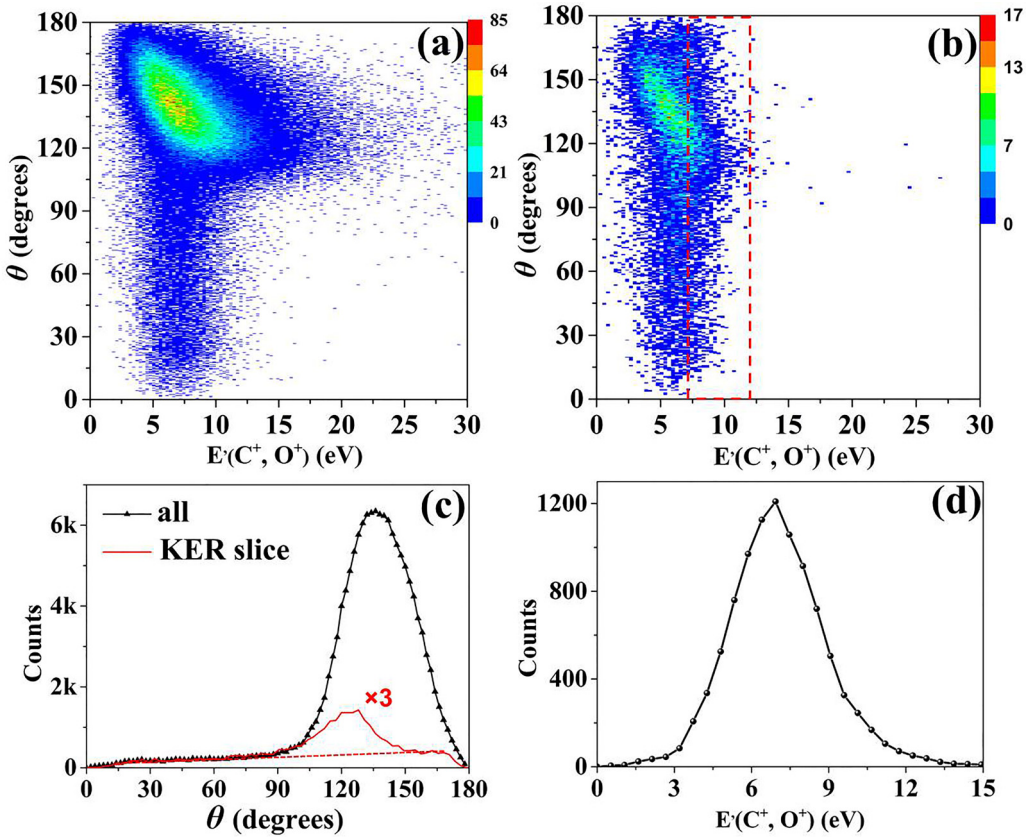

FIG. 5. (a) and (b) A density plot of $O^+ + C^+ + S^{2+}$ events as a function of the kinetic energy of C^+ and O^+ in their c.m. reference $E'(C^+, O^+)$ and θ in the sequential dissociation process for (a) all events and (b) events with low KER restriction, KER < 32 eV, and the gate used to select the sequential breakup events is marked as a red box. (c) Projection of (a) on the angular axis θ for all events (solid-black line) and events (solid-red line) within a red box, and the dotted line represents the fitting line of the counting of sequential dissociation process with the change in θ. (d) KER spectrum for the breakup of CO^{2+} into $C^+ + O^+$ during the second step of the sequential dissociation of OCS^{4+} obtained by partial projection of (a) on the $E'(C^+, O^+)$ axis for $\theta < 90^\circ$.

to excited states with a bending structure before the concerted fragmentation. These values are comparable to the previous measurement obtained in collisions with 1.8-MeV Xe^{9+} [13]. However, in experiment using an intense femtosecond laser, smaller angle between $\vec{p}'_{O^+}$ and $\vec{p}_{S^+}$, $\theta = 120^\circ$, is reported [12]. It shows that for the concerted dissociation of OCS^{3+},

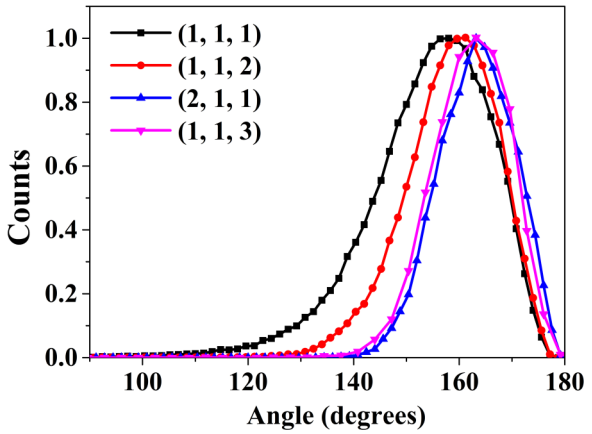

FIG. 6. Angular α between momentum vectors of O^{a+} and S^{c+} ions for the concerted dissociation of charged molecules $OCS^{3,4,5+}$.

the bending structure of the molecule is slightly different depending on the ionization excitation mechanism.

2. *Disentangling sequential from concerted three-body fragmentation of* OCS^{3+} *and* OCS^{4+}

For the sequential dissociation process, under the hypothesis that the contribution of the transverse momentum component due to the rotation of OC^{2+} to $\vec{p}'_{O^+}$ and $\vec{p}'_{C^+}$ is negligible. The kinetic-energy $E'(C^+, O^+)$ in the c.m. of the ensemble C^+ and O^+ corresponds to the KER associated with the second step of dissociation of the intermediate CO^{2+}. From Figs. 5(a) and 7(b) one can see clearly that for $\theta > 90^\circ$ the contribution from sequential dissociation events are overlapped with that of concerted dissociation, whereas for $\theta < 90^\circ$ only sequential events are concerned. By the projection of Figs. 5(a) and 7(b) on the $E'(C^+, O^+)$ axis in the angle region $<90^\circ$, the $E'(C^+, O^+)$ distribution for the dissociation of the intermediate CO^{2+} are obtained and shown in Figs. 5(d) and 7(d). These KER spectra extend from 3 to 12 eV with peaks at ~7.0 and 6.9 eV in the case of OCS^{4+} and OCS^{3+}, respectively. In previous studies on OCS^{3+} sequential dissociation via CO^{2+} for channel (1, 1, 1), Rajput *et al.* [12] and Kumar *et al.* [13] have reported KER distributions for the second step dissociation process $CO^{2+} \rightarrow C^+ + O^+$ centered

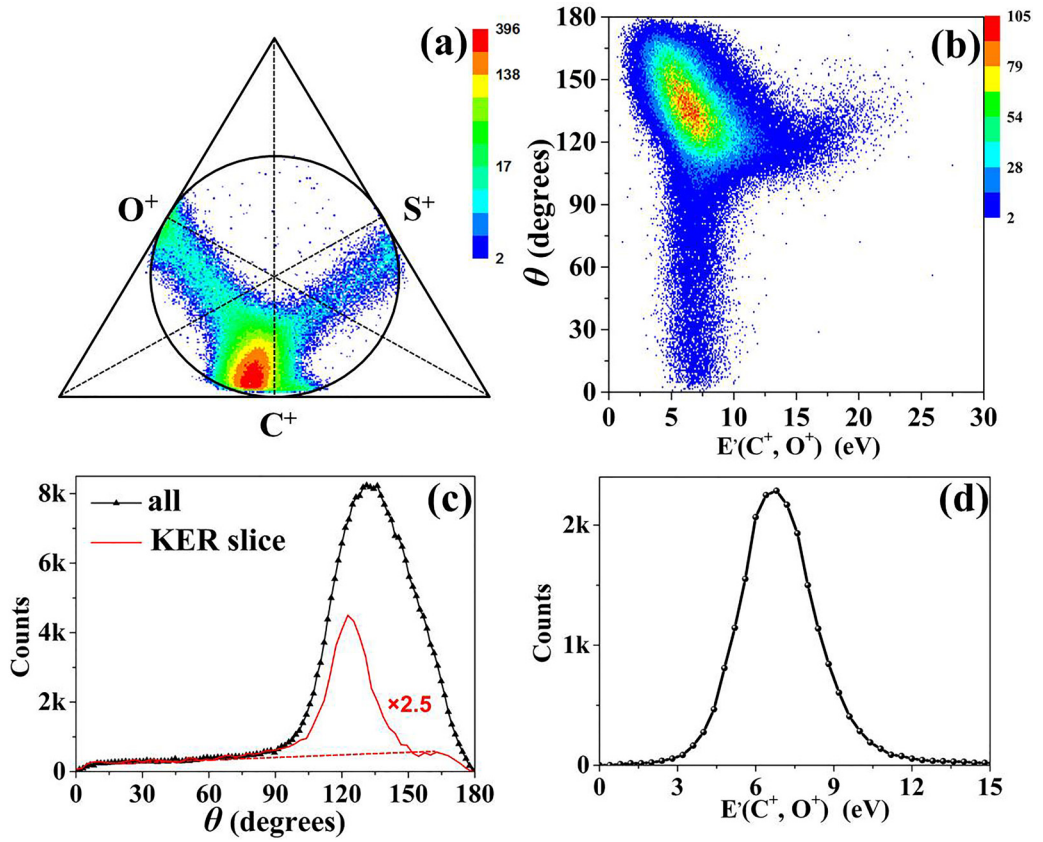

FIG. 7. (a) Dalitz plot for channel (1, 1, 1). (b) A density plot of $O^+ + C^+ + S^+$ events as a function of the kinetic energy of C^+ and O^+ in their c.m. reference $E'(C^+, O^+)$ and θ, and θ represents the angle between $\vec{p}'_{O^+}$ and $\vec{p}'_{S^+}$. (c) Projection of (b) on the angular axis θ (the black line), and the dotted line represents the fitting line of the sequence dissociation process count. (d) KER spectrum for the breakup of CO^{2+} into $C^+ + O^+$ during the second step of the sequential dissociation of OCS^{3+} obtained by partial projection of (a) on the $E'(C^+, O^+)$ axis for $\theta < 90^\circ$.

around 6.5 and 7.5 eV, respectively. The agreement of our results measured in channels (1, 1, 1) and (1, 1, 2) suggests that intermediate CO^{2+} ions in sequential dissociation processes are prepared in molecular states in a comparable energy range quite independent of the first step dissociation. Excited states of CO^{2+} in this energy region have been determined with the help of the KER analyses in the CO^{2+} fragmentation experiments [11,31]. According to the previous experimental and theoretical results, the following electronic states may be involved in the second step dissociation of CO^{2+} : $X\ ^3\Pi$, $^1\Pi$, and $^3\Sigma^+$. Furthermore, the KER distributions for the three-body sequential dissociation of the channel (1, 1, 1) and (1, 1, 2) are found to be centered around 18 and 32 eV in Fig. 8, corresponding to the lower-energy part of the total KER distribution in Fig. 2(a).

In Figs. 5(c) and 7(c), the angle part $\theta < 90^\circ$ is exclusively due to the sequential dissociation. A slow count increase with the angle with the increase can be noted in both cases. To see the evolution of the count-angular distribution in a wider range for sequential dissociation, one has to get rid of the large contribution of the concerted dissociation around 140 °. Taking advantage of the fact that the sequential dissociation occurs mainly in the low KER range, we have built reduced density plots with a restriction in the KER, <32 eV for OCS^{4+} in Fig. 5(b) and <18 eV for OCS^{3+} (not shown here). Therefore, in the regions $\theta_{CO,S} > 160^\circ$ and $E'(C^+, O^+) > 7$ eV, the contribution of the concerted dissociation process can be considered as negligible. The projection on the θ axis of corresponding reduced density plots in a selected energy slice $7\,\text{eV} < E'(C^+, O^+) < 12\,\text{eV}$ are presented in Figs. 5(c) and 7(c), respectively (the red line). Following the count evolution with the angle increasing, a steady increase can be noted

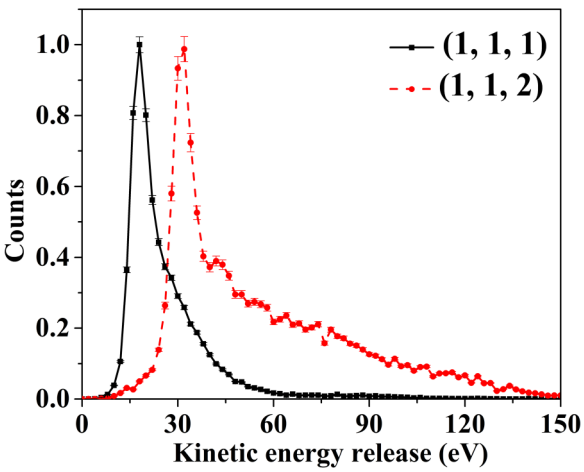

FIG. 8. The KER distributions for the three-body sequential dissociation of channels (1, 1, 1) and (1, 1, 2) via the CO^{2+} intermediate ion.

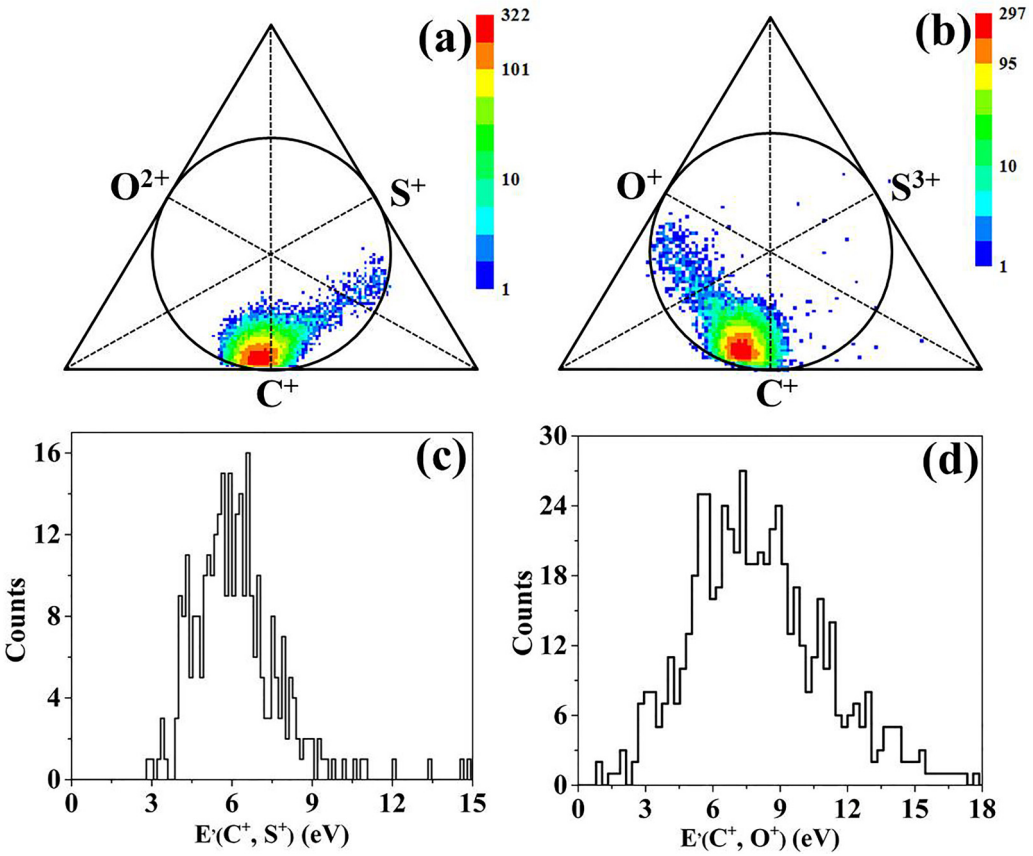

FIG. 9. (a) and (b) Dalitz plot for channels (2, 1, 1) and (1, 1, 3). (c) KER spectrum for the breakup of CS^{2+} into $C^+ + S^+$ during the second step of sequential dissociation of OCS^{4+}. (d) KER spectrum for the breakup of CO^{2+} into $C^+ + O^+$ during the second step of sequential dissociation of OCS^{5+}.

for both OCS^{3+} and OCS^{4+} parent ions. In previous works [12,13], a uniform angular distribution is observed in the sequential dissociation of OCS^{3+} via CO^{2+}. It is the case when the lifetimes of the intermediate CO^{2+} are much larger than the rotation period of the molecule. Indeed, the lifetime of one of the possibly involved state $X\ ^3\Pi$ depends sensibly on the vibration quantum number, ranging from picoseconds to several hundreds of picoseconds. On the other hand, the rotation period τ_R of CO^{2+} depends on the rotation quantum number J, for $J = 1$, $\tau_R = 8$ ps [30,32,33]. In the present paper, due to the different excitation mechanism using highly charged ions instead of the femmtosecond laser, the $E'(C^+, O^+)$ distribution presents a shift to a larger energy value, centered on 7 eV instead of 6.5 eV. Therefore, states of the larger vibration quantum number with a shorter lifetime may be populated. In the case when the lifetime of the molecule is comparable to τ_R and considering the fact that the first half period of CO^{2+} rotation corresponds to the variation of $\theta_{CO,S}$ from the initial maximum value to 0°, a dissociation event count decay as a function of decreasing $\theta_{CO,S}$ is expected. So, the angular dependence of the sequential dissociation count observed in this paper can be interpreted by a partial population of CO^{2+} vibrational states with a larger quantum number and a shorter lifetime in the two-step dissociation of OCS^{3+} and OCS^{4+} prepared in our ion impact experiment.

The number of concerted and sequential events is obtained from Figs. 5(c) and 7(c). The ratio for the breakup of OCS^{3+} via concerted and sequential dissociation is found to be about 0.79:0.21. The ratio for the breakup of OCS^{4+} is found to be about 0.84:0.16. The ratio of sequential dissociation events for OCS^{4+} is lower than that for OCS^{3+}. The reason is that the higher charge state usually means more excitation energy and, thus, less metastable states.

3. *Concerted dissociation and sequential breakup of* OCS^{4+} *via* $CS^{2+} + O^{2+}$ *and* OCS^{5+} *via* $CO^{2+} + S^{3+}$

The experimental Dalitz plots [cf. Figs. 9(a) and 9(b)] for channels (2, 1, 1) and (1, 1, 3) show very similar signatures compared with that for channel (1, 1, 2). The intense spot near the edge (C^+) corresponding to the concerted dissociations $OCS^{4+} \rightarrow O^{2+} + C^+ + S^+$ and $OCS^{5+} \rightarrow O^+ + C^+ + S^{3+}$. In the corresponding region, angle α between the measured momentum vectors of O^{2+} and S^+ is found to be about 160° for channel (2, 1, 1), a nearly same angle is found between the momentum vectors of O^+ and S^{3+} for channel (1, 1, 3) in Fig. 6. For both cases, the contribution from OCS^{4+} and OCS^{5+} with the bending structure before the concerted dissociation is dominant comparing to the linear structure. Clear winglike structures can be noted in Figs. 9(a) and 9(b) which correspond to the sequential breakup processes. Different from the two-wing structure as in Fig. 7(a), only one wing is present in each of the Dalitz plots. From the strong momentum correlation between C^+ and S^+ shown in Fig. 9(a) and between O^+ and C^+ in Fig. 9(b), we can conclude that the

sequential breakup of channels (2, 1, 1) and (1, 1, 3) occurs only via CS^{2+} and CO^{2+}, respectively, intermediate molecular ions.

Comparing with the channels analyzed in the previous sections, the counts of the two channels (2, 1, 1) and (1, 1, 3) are too small to allow for the angular analysis with the native frame. The $E'(C^+, S^+)$ distribution of the second step in the sequential dissociation of OCS^{4+}, $CS^{2+} \rightarrow C^+ + S^+$ is obtained by analyzing selectively events in the winglike part of the Dalitz plot in Fig. 9(a). Shown in Fig. 9(c), it extends from 3 to 11 eV with a peak at ~6.0 eV. This peak value is almost the same as in the (1, 1, 1) sequential dissociation channel via the CS^{2+} intermediate ion measured in previous works [12,13]. Based on the kinetic-energy release data, the CS^{2+} molecular ions are populated most probably around the state $X\ ^3X_{\upsilon=13}$ [34] before dissociation.

Similarly, the $E'(C^+, O^+)$ spectra of the second step in the sequential dissociation of OCS^{5+}, $CO^{2+} \rightarrow O^+ + C^+$ is shown in Fig. 9(d). It is generated by analyzing selectively events in the winglike part of the Dalitz plot in Fig. 9(b). This $E'(C^+, O^+)$ distribution extends from 2 to 16 eV with a peak around ~7.5 eV. Based on theoretical results by Lundqvist *et al.* [31], the contributing states of CO^{2+} could be $X\ ^3\Pi$, $^1\Pi$, $^3\Sigma^+$, and 2 $^1\Sigma^+$ (range from 7.6 to 9.5 eV). Comparing the $E'(C^+, O^+)$ distributions measured in sequential dissociation of parent molecular ions OCS^{q+} with different charge states, $q = 3$–5 via the CO^{2+} intermediate ion, one can note that the $E'(C^+, O^+)$ peak values for the dissociation process $CO^{2+} \rightarrow O^+ + C^+$ are very similar and independent of the first step dissociation and the charge of the parent molecular ions.

Apart from the four channels analyzed above, (1, 1, 1), (1, 1, 2), (2, 1, 1), and (1, 1, 3), no trace of a sequential mechanism is observed for the remaining six dissociation channels listed in Table I. By comparing the dissociation products of all three-body channels in Table I, it can be inferred that the sequential dissociation process occurs when the CO^{2+} or CS^{2+} intermediate ions could be formed in the first step, but metastable states of CO^{q+} or CS^{q+} intermediate ions have never been observed for $q > 2$. This is probably due to the fact that these higher charged diatomic ions are prepared in dissociative states and the parent molecules could only undergo concerted dissociation.

IV. SUMMARY

In the present paper, the fragmentation dynamics of the OCS molecule in collision with 18-keV/u Ne^{8+} ions beam was studied using the COLTRIMS technique. The three-dimensional momenta of all recoil ions were reconstructed. Ten three-body Coulomb explosion channels resulting from the dissociation of OCS^{q+} ($q = 3$–7) were analyzed using the triple ion coincidence map. For each channel, branching ratios were provided, and the kinetic-energy release of the fragmentation was compared to the Coulomb explosion model. The evolution of KER values obtained within a simple CEM was found in good agreement with the experimental data. The correlation between the final projectile charge state and the KER was briefly discussed. Furthermore, dissociation mechanisms in three-body fragmentation channels of OCS^{q+} ($q = 3$–7) were analyzed using Dalitz plots, Newton diagrams, and native frames. Both concerted dissociation and sequential breakups of OCS^{q+} ($q = 3$–5) via CO^{2+} or CS^{2+} were observed in the following channels: $OCS^{3+} \rightarrow CO^{2+} + S^+ \rightarrow O^+ + C^+ + S^+$, $OCS^{4+} \rightarrow CO^{2+} + S^{2+} \rightarrow O^+ + C^+ + S^{2+}$, $OCS^{4+} \rightarrow O^{2+} + CS^{2+} \rightarrow O^{2+} + C^+ + S^+$, and $OCS^{5+} \rightarrow CO^{2+} + S^{3+} \rightarrow O^+ + C^+ + S^{3+}$. For concerted dissociation, we found evidence for a bending of the molecule prior dissociation. The sequential dissociation events were all found related to the dissociation of metastable intermediate ions CO^{2+} or CS^{2+}. The KER distributions for the dissociation of CO^{2+} or CS^{2+} were deduced, and the corresponding excited states were identified. Furthermore, in sequential dissociation channels involving CO^{2+}, the angular distribution was found with a slight anisotropy, which was interpreted as a result of the very short lifetime CO^{2+} in the two-step dissociation of OCS^{3+} and OCS^{4+}.

ACKNOWLEDGMENTS

This work was supported by the National Key Research and Development Program of China under Grant No. 2017YFA0402300 and the National Natural Science Foundation of China under Grants No. U1832201 and No. 11674067.

[1] R. K. Janev and D. Reiter, Contrib. Plasma Phys. **50**, 986 (2010).
[2] R. Thissen, O. Witasse, O. Dutuit, C. S. Wedlund, G. Gronoff, and J. Lilensten, Phys. Chem. Chem. Phys. **13**, 18264 (2011).
[3] M. R. Swain, G. Vasisht, and G. Tinetti, Nature (London) **452**, 329 (2008).
[4] U. Werner, K. Beckord, J. Becker, and H. O. Lutz, Phys. Rev. Lett. **74**, 1962 (1995).
[5] A. Hishikawa, H. Hasegawa, and K. Yamanouchi, Chem. Phys. Lett. **361**, 245 (2002).
[6] C. Wu, C. Wu, D. Song, H. Su, Y. Yang, Z. Wu, X. Liu, H. Liu, M. Li, Y. Deng, Y. Liu, L.-Y. Peng, H. Jiang, and Q. Gong, Phys. Rev. Lett. **110**, 103601 (2013).
[7] S. Hsieh and J. H. D. Eland, J. Phys. B: At., Mol. Opt. Phys. **30**, 4515 (1997).
[8] J. Ullrich, R. Moshammer, A. Dorn, R. Dörner, L. P. H. Schmidt, and H. Schmidt-Böcking, Rep. Prog. Phys. **66**, 1463 (2003).
[9] N. Neumann, D. Hant, L. P. H. Schmidt, J. Titze, T. Jahnke, A. Czasch, M. S. Schöffler, K. Kreidi, O. Jagutzki, H. Schmidt-Böcking, and R. Dörner, Phys. Rev. Lett. **104**, 103201 (2010).
[10] E. Wang, X. Shan, Z. Shen, M. Gong, Y. Tang, Y. Pan, K.-C. Lau, and X. Chen, Phys. Rev. A **91**, 052711 (2015).
[11] S. Yan, X. L. Zhu, P. Zhang, X. Ma, W. T. Feng, Y. Gao, S. Xu, Q. S. Zhao, S. F. Zhang, D. L. Guo, D. M. Zhao, R. T. Zhang, Z. K. Huang, H. B. Wang, and X. J. Zhang, Phys. Rev. A **94**, 032708 (2016).

[12] J. Rajput, T. Severt, B. Berry, B. Jochim, P. Feizollah, B. Kaderiya, M. Zohrabi, U. Ablikim, F. Ziaee, K. Raju P., D. Rolles, A. Rudenko, K. D. Carnes, B. D. Esry, and I. Ben-Itzhak, Phys. Rev. Lett. **120**, 103001 (2018).
[13] H. Kumar, P. Bhatt, C. P. Safvan, and J. Rajput, J. Chem. Phys. **148**, 064302 (2018).
[14] L. Leman, L. Orgel, and M. R. Ghadiri, Science **306**, 283 (2004).
[15] J. H. Sanderson, T. R. J. Goodworth, A. El-Zein, W. A. Bryan, W. R. Newell, A. J. Langley, and P. F. Taday, Phys. Rev. A **65**, 043403 (2002).
[16] W. A. Bryan, W. R. Newell, J. H. Sanderson, and A. J. Langley, Phys. Rev. A **74**, 053409 (2006).
[17] V. Brites, J. H. D. Eland, and M. Hochlaf, Chem. Phys. **346**, 23 (2008).
[18] B. Wales, E. Bisson, R. Karimi, S. Beaulieu, A. Ramadhan, M. Giguere, Z. J. Long, W. K. Liu, J. C. Kieffer, F. Legare, and J. Sanderson, J. Electron Spectrosc. Relat. Phenom. **195**, 332 (2014).
[19] K. Saha, S. Banerjee, and B. Bapat, Chem. Phys. Lett. **607**, 85 (2014).
[20] P. Wang and C. R. Vidal, J. Chem. Phys. **118**, 5383 (2003).
[21] Z. Shen, E. Wang, M. Gong, X. Shan, and X. Chen, J. Chem. Phys. **145**, 234303 (2016).
[22] M. R. Jana, B. Ray, P. N. Ghosh, and C. P. Safvan, J. Phys. B: At., Mol. Opt. Phys. **43**, 215207 (2010).
[23] M. R. Jana, P. N. Ghosh, B. Ray, B. Bapat, R. K. Kushawaha, K. Saha, I. A. Prajapati, and C. P. Safvan, Eur. Phys. J. D **68**, 250 (2014).
[24] B. Wales, T. Motojima, J. Matsumoto, Z. Long, W.-K. Liu, H. Shiromaru, and J. Sanderson, J. Phys. B: At., Mol. Opt. Phys. **45**, 045205 (2012).
[25] Y. Zhang, T. Jiang, L. Wei, D. Luo, X. Wang, W. Yu, R. Hutton, Y. Zou, and B. Wei, Phys. Rev. A **97**, 022703 (2018).
[26] R. A. Phaneuf, F. W. Meyer, and R. H. McKnight, Phys. Rev. A **17**, 534 (1978).
[27] P. Ma, C. Wang, S. Luo, X. Yu, X. Li, Z. Wang, W. Hu, J. Yu,Y. Yang, X. Tian, Z. Cui, and D. Ding, J. Phys. B: At., Mol. Opt. Phys. **51**, 094002 (2018).
[28] A. Khan, L. C. Tribedi, and D. Misra, Phys. Rev. A **96**, 012703 (2017).
[29] F. Penent, R. I. Hall, R. Panajotović, J. H. D. Eland, G. Chaplier, and P. Lablanquie, Phys. Rev. Lett. **81**, 3619 (1998).
[30] J. P. Bouhnik, I. Gertner, B. Rosner, Z. Amitay, O. Heber, D. Zajfman, E. Y. Sidky, and I. Ben-Itzhak, Phys. Rev. A **63**, 032509 (2001).
[31] M. Lundqvist, P. Baltzer, D. Edvardsson, L. Karlsson, and B. Wannberg, Phys. Rev. Lett. **75**, 1058 (1995).
[32] F. Mrugała, J. Chem. Phys. **129**, 064314 (2008).
[33] T. Šedivcová, P. R. Žďánská, and V. Špirko, J. Chem. Phys. **124**, 214303 (2006).
[34] T. Šedivcova, V. Špirko, and J. Fišer, J. Chem. Phys. **125**, 164308 (2006).